Yang, X.; Zhao, L.; Almasy, L.; Garamus, V.M.; Zou, A.;
Willumeit, R.; Fan, S.:

Preparation and characterization of 4-dedimethylamino sancycline (CMT-3) loaded nanostructured lipid carrier (CMT-3/NLC) formulations

In: International Journal of Pharmaceutics (2013) Elsevier

DOI: 10.1016/j.ijpharm.2013.04.021

Preparation and characterization of 4-dedimethylamino sancycline (CMT-3) loaded nanostructured lipid carrier (CMT-3/NLC) formulations

Xiaomin Yang[1a] Lin Zhao[1c] Laszlo Almasy[d] Vasil M. Garamus[b] Aihua Zou[*a] Regine Willumeit[b] Saijun Fan[c]

[a]State Key Laboratory of Bioreactor Engineering and Institute of Applied Chemistry, East China University of Science and Technology, Shanghai 200237, PR China,

[b]Helmholtz-Zentrum Geesthacht: Centre for Materials and Coast Research, Institute of Materials Research, Max-Planck-Str. 1, D-21502 Geesthacht, Germany

[c]School of Radiation Medicine and Protection, Soochow University Medical College, Suzhou 215123, PR China

[d] Research Institute for Solid State Physics and Optics, HAS, Konkoly-Thege Miklós út 29-33, 1525 Budapest, Hungary

* To whom correspondence should be addressed. Tel/Fax.: +86-21-64252063.

E-mail: aihuazou@ecust.edu.cn.

[a]East China University of Science and Technology.

[b]Helmholtz-Zentrum Geesthacht.

[c]Soochow University Medical College

Abstract

Chemical modified tetracyclines (CMTs) have been reported to have strong inhibition ability on proliferation and invasion of various cancers, but its application is restricted for its poor water solubility. In present study, hydrophilic CMT-3 loaded nanostructured lipid carrier (CMT/NLC) was produced by high pressure homogenization (HPH). The physical properties of CMT/NLC were characterized by dynamic light scattering (DLS), high efficiency liquid chromatography (HPLC), atomic force microscopy (AFM), Scan electron microscopy (SEM), Small-Angle Neutron Scattering (SANS), small angle and wide angle X-ray scattering (SAXS and XRD) The lipids and surfactants ingredients, as well as drug/lipids (m/m) were investigated for stable and sustained NLC formulations. In vitro cytotoxicity of CMT/NLC was evaluated by MTT assay against HeLa cells. The diameter of CMT/NLC increased from 153.1±3.0 nm to maximum of 168.5±2.0 nm after 30 days of storage while the entrapment efficiency kept constant at ＞90 %. CMT/NLC demonstrated burst-sustained release profile in release mediums with different pH, and the 3-dimension structure of CMT/NLC was suspected to attribute this release pattern. The results of cell uptaking and location indicated that NLC could arrive at cytoplasm and NLC makes CMT-3 entering HeLa cells easier. All results showed that NLC was important to CMT-3 application not only in lab research but also in clinical field. To the best of our knowledge this is the first report on CMT/NLC.

Key words: Nanostructured lipid carriers; CMT-3; SANS&SAXS; XRD; in-vitro

release; cytotoxicity

1. Introduction

Chemically modified tetracyclines (CMTs) are analogs of tetracycline (Fig 1), which is used clinically as an antibiotic agent. Golub and co-workers first investigated and described that CMTs lack antimicrobial properties but still inhibit matrix metalloproteinases (MMPs) (Golub et al., 1991). Since then, numerous in vivo and in vitro studies have demonstrated that CMT-3, also known as COL-3, is the most promising anti-tumor molecular compared to other CMTs (Lokeshwar et al., 2002). CMT-3 has been shown to have strong inhibition ability on proliferation and invasion of various cancer, such as E-10, MDA-MB-468 human breast cancer cells, COLO 205 colon carcinoma cells, and DU-145, TSU-PR1, and Dunning MAT LyLu human prostate cancer cells (Gu et al., 2001; Lokeshwa, 1999; Lokeshwa et al., 1998; Lokeshwar et al, 2001; Lokeshwar et al, 2002; Meng et al., 2000). The anti-metastatic effect of CMT-3 also has been assessed in the bone metastasis model of MAT LyLu human prostate cancer cells in rats and the lung metastasis model of C8161 human melanoma cells in SCID mice (Seftor et al., 1998; Selzer et al., 1999). Though CMT-3 had significant effect on inhibiting tumor metastasis and had several potential advantages over conventional tetracyclines, the adverse effects included nausea, vomiting, liver function tests abnormalities, diarrhea, mucositis, leukopenia, and thrombocytopenia were observed in clinical trials (Syed et al., 2004). The main reason may attribute to CMT-3's hydrophobic and lipophilic ability, which make it concentrate in high fatty tissue and produce toxic effects. Because of the poor

water-solubility, the drug is hard to be absorbed into human blood and interstitial fluid, and it is difficult to be transported into the target human body or abnormal tissue and organ effectively. On the other hand, because CMT-3 can't be dissolved totally in saline, the injection manner of giving drug may be forbidden in clinical usage. So, the improvement of CMT-3 water-solubility has great importance in its clinic application.

Fig 1. The structures of doxycycline (upper) and CMT-3 (lower).

Over the past several decades, much interest has focused on the design of more efficient drug delivery systems to address problems such as low drug solubility. The particulate delivery systems address a number of characteristics including appropriate size distribution, high drug loading, prolonged release, low cellular cytotoxicity and cellular targeting. The nanostructured lipid carrier was first developed by Prof. Rainer H. Müller during the late 1990s (Eliana et al., 2010). NLC is composed of mixture of solid and liquid lipid compounds such as triacylglycerols, fatty acids, steroids, and oil (Rainer et al., 2007). NLC is attractive for its combination of advantages of many other drug carriers (solid lipid nanoparticles, polymeric nanoparticles, liposomes and emulsions) (Rainer et al., 2004). NLC can be produced on a large scale using lipids and surfactants that are already accepted, and long-term stability NLC formulations have been reported for various applications (Khalil et al., 2011; Medha et al., 2009). NLC can enhance lipophilic drug solubility by virtue of its lipids core and aqueous shell. Enhances solubility is significant because a great number of drug candidates are poorly soluble. Also, the solid matrix provides NLC with sustained release properties, as the degradation or erosion of the lipid matrix releases the incorporated drugs from

NLC. Finally, the nanosize of NLC increases its therapeutic efficacy and reduces toxicity. In this study, CMT-3 was incorporated into a NLC made up of biodegradable and biocompatible fatty acids and triacylglycerols. The aim of this study was to design long-term stable ~~water soluble~~ CMT/NLC formulations with proper size, high drug loading and sustained release profiles. Cellular uptake and cellular location were investigated using rhodamine B as a probe for these high efficiency antitumor formulations. To our knowledge, this is the first repot on CMT/NLC, and there has no evidence showing CMT-3 loaded other nanoformulations so far. The results in this study imply that this CMT-3 loaded nanocarrier may significantly improve the effectiveness of CMT-3 in clinical applications.

2. Materials and methods

2.1 Materials

4-dedimethylamino sancycline (CMT-3, CollaGenex Pharmaceuticals Inc, Newtown, Pennsylvania); Steric acid (SA, LingFeng Chemical Reagent Co. Ltd, China); monoglyceride (MGE, Aladdin Chemical Reagent Co. Ltd, China); oleic acid (OA, Aladdin Chemical Reagent Co. Ltd, China); capric/caprylic triglycerides (MCT, Aladdin Chemical Reagent Co. Ltd, China); Cremophor EL(Aladdin Chemical Reagent Co. Ltd, China); Pluronic F68 (Adamas Reagent Co. Ltd, China); freshly prepared double distilled and ultra purified water; trehalose (Aladdin Chemical Reagent Co. Ltd, China); 3-(4,5-dimethylthiazol-2-yl)-2,5-diphenyltetrazolium

bromide (MTT, Sigma-Aldrich, MO, USA), D_2O (Sigma, Germany).

2.2. Preparation, particle sizes and size distribution of NLCs

NLC were prepared by high pressure homogenizer (HPH). In brief, aqueous phase which consisted of double distilled water and one or two surfactants mixture(1/1, m/m) and oil phases (lipid mixtures, including SA, MGE, OA and MCT) were separately prepared. Desired oil phase were maintained at 70 °C to prevent the recrystallization of lipids during the process, then CMT-3 was added to the oil phase which was stirred until completely dissolved. The same temperature aqueous phase was added to the oil phase with intense stirring (10000 rmp for 1 min; Turrax T25, Fluko, Germany). These dispersions were processed through an HPH (ATS Engineering, Canada) with five homogenization cycles at 600 bar. The nanodispersions were cooled overnight at room temperature to obtain the nanostructure lipid carrier.

All samples were lyophilized for long stability. Appropriate amounts of trehalose (3% w/v in water) were used to dilute the NLC dispersions. The samples were frozen at -78 °C for 10 h before being lyophilized for 36 h. The freeze-dried powders were rehydrated with phosphate buffer solution (PBS, pH 7.4) for later experiments.

The mean particle size and polydispersity of NLCs were measured by dynamic light scattering at 25 °C using Nano-ZS90 system (Malvern Instruments Ltd., UK) with a measurement angle of 90 °.

2.3. Entrapment efficiency (EE) and drug loading (DL)

To determine the amount of CMT-3, methanol was added to CMT/NLC formulations to destroy the NLC structure and dissolve the CMT-3 that was released. The content of CMT-3 was determined by HPLC (Wufeng, China) using the following experiment conditions: Diamond C18 column (150 nm×4.6 nm i.d, pore size 5μm; A yi te, China), the mobile phase MeOH: H_2O (0.5% TFA, v/v) = 30:70 (v/v), flow rate: 1 mL/min, and wavelength: 360 nm. The calibration curve of CMT-3 concentration against peak area was $C=8.86793*10^{-7}A+0.00248$ ($R^2=0.9999$). All the experiments were conducted at room temperature (25 °C). The drug loading (DL%) and entrapment efficiency (EE%) were calculated by the following formulas:

DL% = the weight of CMT-3 encapsulated in the NLC / the total weight of CMT/NLC ×100;

EE% = the calculated DL / the theoretical DL ×100.

2.4. NLC morphology study

The surface morphology of NLCs was examined by Nanofirst-3100 AFM (Suzhou Hai Zi Si Nanotechnology Ltd, China). Samples for AFM were prepared by placing a drop of freshly prepared unloaded blank-NLC and CMT/NLC on the mica sheet and drying by spin coating.

Scan electron microscopy (SEM, Auriga 40, Zeiss, Germany) was used to study the internal structures of blank-NLC and CMT/NLC. Before scanning, the samples were placed on the conductive double-sided sticky tape and then coated with gold in an argron atmosphere.

155 *2.5. Small-Angle Neutron Scattering*

156 SANS measurements were performed on the Yellow Submarine instrument at the
157 BNC in Budapest (Hungary) (Rosta L, 2002). The overall q-range was from 0.03 to 1
158 nm^{-1}. The samples were filled in Hellma quartz cells of 2 mm path length and placed
159 in a thermostated holder kept at 20.0±0.5 °C. The raw scattering patterns were
160 corrected for sample transmission, room background, and sample cell scattering. The
161 2-dimensional scattering patterns were azimuthally averaged, converted to an absolute
162 scale and corrected for detector efficiency dividing by the incoherent scattering
163 spectra of 1 mm thick pure water. The scattering from PBS buffer prepared in D_2O
164 was subtracted as the background. Fourier Transformation (IFT) was applied in this
165 study to analyse the scattering pattern.

166 2.6. *Small-Angle X-Ray Scattering*

167 The SAXS measurements were performed at laboratory SAXS instrument
168 (Nanostar, Bruker AXS GmbH, Karlsruhe, Germany). Instrument includes IμS
169 micro-focus X-ray source with power of 30 W (used wavelength Cu Kα) and
170 VÅNTEC-2000 detector (14×14 cm^2 and 2048×2048 pixels). Sample to detector
171 distance is 108.3 cm and accessible q range from 0.1 to 2.3 nm^{-1}.

172 *2.7. Wide-Angle X-ray powder diffraction*

173 The crystalline structure of CMT-3, unloaded blank-NLC and CMT/NLC were
174 investigated by D/MAX 2550 VB/PC X-ray diffractometry (Rigaku, Japan). Aqueous
175 blank-NLC and CMT/NLC were lyophilized before the XRD measurement.

Diffractograms were obtained from the initial angle 2 θ = 10 ° to the final angle 60 ° with a Cu Kα radiation source. The obtained data were collected with a step width of 0.02 ° and a count time of 1 s.

2.8. In vitro release of CMT-3

The in vitro release of CMT-3 from CMT/NLC was conducted by dialysis bag diffusion (Xu et al., 2009). 5 mL fresh prepared CMT/NLC solution (100 μg/ml) was placed into a pre-swelled dialysis bag with 7 KDa MW cutoff. The dialysis bag was incubated in release medium (PBS, pH 7.4 VS pH 5.5; 20 mL) with 0.5 % of Tween 80 to enhance the solubility of released free CMT-3 and to avoid its aggregation at 37 ℃ under horizontal shaking. At predetermined time points, the dialysis bag was taken out and placed into a new container containing fresh release medium (20 mL). The content of CMT-3 in release medium was determined by HPLC as described by section 2.3. The release rates of CMT-3 were expressed as the mass of CMT-3 in release medium divided by time.

2.9. Cell morphology

HeLa cells were seeded in 6-well plate after 0.25 % trypsin digestion at a density of 3×10^6 per well. After 12 h, cells were exposed to 20 μM CMT-3, blank-NLC and CMT/NLC for 6 h. The cell morphology was captured by digital camera (Olympus).

2.10. Cell culture

The human cervical cancer cell line HeLa was purchased from American Type Culture Collection (Manassas, VA, USA). The cells were seeded into cell culture

dishes containing DMEM supplemented with 10 % new calf serum, *L*-glutamine (5 mmol/L), non-essential amino acids (5 mmol/L), penicillin (100 U/mL), and streptomycin (100 U/mL) (Invitrogen, Carlsbad, CA, USA), at 37 °C in a humidified 5% CO_2 atmosphere.

2.11. In vitro cellular cytotoxicity assays

Cell viability was measured by 3-(4,5-dimethylthiazol-2-yl)-2,5-dipheny ltetrazoliumbromide (MTT) assay. HeLa cells were plated in 96-well plates with 100 μL medium at a density of 8×10^3 per well. After 12 h, cells were exposed to various concentrations of CMT-3, blank-NLC and CMT/NLC for 24 and 48 h. MTT solution was directly added to the media in each well, with a final concentration of 0.5 mg/mL and incubated for 4 h at 37 °C. The formazan crystals were solubilized with 150 μL DMSO. The absorbance was measured using an enzyme-linked immunosorbent assay reader at 570 nm, with the absorbance at 630 nm as the background correction. The effect on cell proliferation was expressed as the percent cell viability. Untreated cells were taken as 100 % viable.

2.12. Cellular uptake of NLC formulations

Rhodamine B (RB, Sigma-Aldrich, MO, USA) was used as probe to study the uptake and location of NLC in Hela cells. RB was encapsulated in NLC, and the free RB was removed via dialysis bag (MW 7000). HeLa cells were seeded in Lab Tek chamber slides (Nunc, Wiesbaden, Germany) at the density of 2×10^4 and incubated for 24 h. The real-time subcellular localization was determined using Cell'R Live Cell Station (Olympus Company, Inc). The images were captured every 30 second and last

for 15 min. RB/NLC was added at equivalent rhodamine B immediately after the first image captured.

3. Results and discussion

3.1. Preparation, particle sizes and distribution of NLCs

In this study, monoglyceride and stearic acid (solid lipids) and oleic acid and capric/caprylic triglycerides (liquid lipids) were selected for their high ability to dissolve CMT-3. The non-toxic, non-ionic surfactants, Cremophor EL and Pluronic F68 were used to increase the stability of NLC.

Many methods have been reported for NLC preparation, including hot and cool homogenization (Liu et al., 2010), microemulsion (Soheila et al., 2010), ultrasonication (Wang et al., 2009), solvent emulsion and phase inversion. Among these, hot homogenization and solvent emulsion have been widely applied, and given the point that CMT-3 is easily dissolved in organic solvent, high pressure homogenization (HPH) was used to prepare CMT/NLC for high entrapment efficiency.

Table 1. Effects of lipid ingredients on mean particle size of blank-NLC.

Formula (Lmix-n)	MGE (mg)	SA (mg)	MCT (mg)	OA (mg)	Mean particle size (nm)	PDI*
Lmix-1	1113	557	415	415	190±3.2	0.30
Lmix-2	1113	557	593	237	150±5.0	0.14
Lmix-3	1074	596	553	277	148±1.9	0.15

Lmix-4	1074	596	593	237	138±4.2	0.20

SA (stearic acid) is a saturated fatty acid with an 18 carbon-chain length, and a highly lipophilic character. It is often used as solid lipid for the production of NLC. The selection of MCT as liquid lipid was for its thermodynamic stability, and high solubility for many drugs (Patricia et al., 2011). In addition, its less ordered structure is better for imperfect NLC, which is critical for high EE and DL. In fact, as indicated in Table.1, formulas (Lmix-2 VS Lmix-1, and Lmix-4 VS Lmix-3) with high MCT showed smaller sizes and more uniform dispersion, while the incorporation of OA increased the particle size and PDI. This was mainly because the melting point of OA is low and therefore OA increases the mobility of the internal lipids and fluidity of the surfactant layer (Radheshyam and Kamla, 2011). Consequently, the ratios between lipids were fixed as MGE/SA = 2/1, and CMT/OA = 2/1 (m/m).

Table 2. Effects of the concentration of surfactants on mean particle size and stability.

Total surfactant concentration (%)	Mean particle size (nm)		Stability*
	1 day	10 day	
0.12	133.6±10	276.5±12	+
0.15	143.3±2.3	257.7±5.7	+
0.2	142.0±2.1	157.8±1.2	-
0.3	141.6±7.5	356.2±11.2	-

249 The studies of surfactants are of great importance for the development of stable
250 NLC formulas. In addition, while moving through the vasculature, NLC interacted
251 with various components of blood. The hydrophilic of NLC avoid protein adsorption
252 on the surface and hence induce delayed immune clearance (Yoo. et al., 2011).
253 Cremophor EL is FDA approved, and already clinically used for intravenous injection.
254 In addition, F68 was chosen for its long PEG chains, and PEG chains are known for
255 providing a stealth character to nanocarriers and slow their elimination from the
256 bloodstream during intravenous injection (Delmas et al., 2010).

257 According to pre-experiments (surface tension studies, data are not shown) the
258 ratio between Cremophor EL and F68 was fixed as 1:1. The total surfactant
259 concentration was also studied. As can be seen from Table 2, the concentration of
260 surfactants had only slight effects on mean particle size, whereas increasing
261 concentrations of surfactant had significant influence on the stability of the dispersion.
262 This could be explained by the fact that high amount of surfactant make the oil phase
263 disperse more readily into aqueous phase. Also, the new lipid surface presented during
264 the HPH process was covered by high concentrations of surfactant, thereby providing
265 higher homogenization efficiency. Too much surfactant, however, lowered the
266 stability of NLC. Many factors may have contributed to this phenomenon. For
267 example, the long PEG chains of F68 can interact with each other by hydrogen
268 bonding, and surfactants may form large size micelles.

269 *3.2. Entrapment efficiency and drug loading*

270 Not only the stability, but also entrapment efficiency and drug loading are vital

for clinical application of CMT/NLC. In section 3.1, the type and concentration of lipid ingredients and surfactants were investigated for stable and small size NLC formulas, in this section the effects of the ratio between drug and lipids on entrapment efficiency and drug loading was studied.

Table 3. The effects of lipids and CMT-3 content on mean particle size. Values are mean ± SD (n=3)

Experiments	Lipid content (mg)	CMT-3 content (mg)	1 day	30 day
			Mean particle size (nm)	Mean particle size (nm)
1	807.0	38.5	140.0±3.2	145.7±4.9
2	807.0	60.5	145.8±4.9	154.5±5.0
3	807.0	100.0	145.2±5.0	200.0±3.5
4	1614.0	100.0	153.1±3.0	168.5±2.0
5	1614.0	200.0	142.4±5.1	200.0±4.5

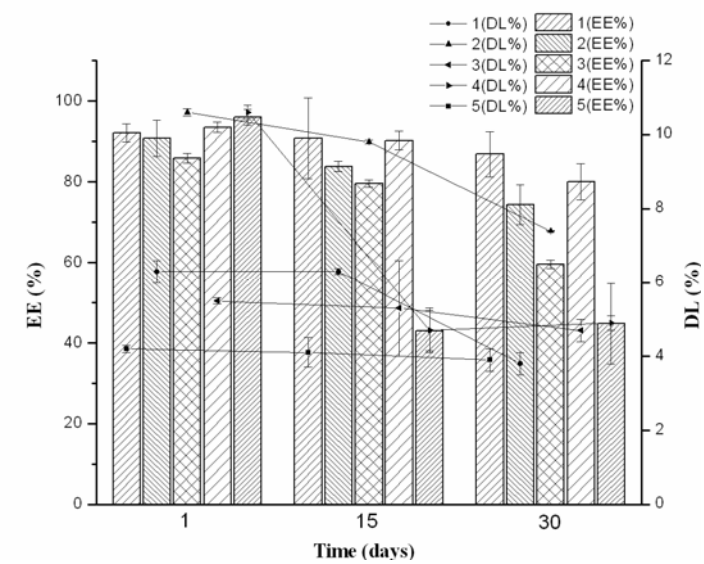

Fig 2. The effects of lipids and CMT-3 concentration on entrapment efficiency and drug loading. *The labels of samples are the same as in Table. 3. Values are mean ± SD (n=3).

The details of CMT/NLC formulas were shown in Table 3, and the mean particle sizes were measured during 30 days. It was clear that the particle sizes of all formulas were ＜200 nm during the storage period. Fig 2 illustrates that the amount of lipids and CMT-3, and the storage time, had direct relationships with the entrapment efficiency and drug loading. For the first day after preparation, the entrapment efficiency and drug loading values of these CMT/NLC formulations (experiments 1 – 5) were in the range of 90 - 96 % and 4.2 - 10.6 %, respectively. It can be concluded from the data for experiments 1, 2 and 3, that higher drug/lipid ratios didn't increase the entrapment efficiency. When the amount of CMT-3 is close to its saturation solubility in the lipid phase, cooling the nanoparticles leads to supersaturation of CMT-3 in the liquid lipids and consequently to CMT-3 precipitation prior to lipid precipitation, and therefore to lower entrapment efficiency (Sylvia and Rainer., 2004).

The entrapment efficiency of experiment 4 was higher than that of experiment 3; this can be explained by the fact that high amounts of lipids increase the solubility of CMT-3. According to the results from Table 3 and Fig 2, the experiment 4 was chosen for further studied.

3.3. NLC morphology study

Given that the shape of NLC may affect important biological processes, including biodistribution and cellular uptake, in drug delivery application (Venkateraman et al., 2011), AFM was used to investigate the non-hydrated state of NLCs. It can be seen from Fig 3 that both blank-NLC and CMT/NLC had irregular morphology with smooth surface. Many factors may induce irregular morphology, for example, i) the powerful mechanical force and shearing force during preparation, ii) liquid lipids increase the mobility of lipid phase. But larger particles may result from the NLC aggregation during spin coating.

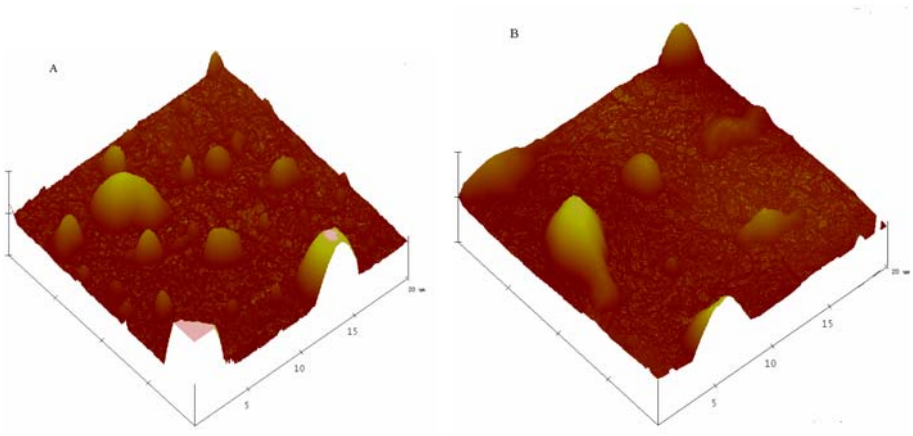

Fig 3. AFM images of blank-NLC (A), and CMT/NLC (B).

Fig 4 demonstrated the SEM results of unloaded NLC and CMT loaded NLC after freeze-drying. Both the blank-NLC and CMT/NLC were located in the bulk and

grid structure formed by trehalose. The diameters of from SEM were larger than those measured by DLS because of the coating before measurement. In addition, the shape of unloaded NLC was almost spherical, but CMT/NLC was elongated. It was reported that the elongated, flexible core-shell structures have demonstrated unique visco-elastic and rheological properties (Ezrahi et. al., 2007; Dreiss, 2007) and the importance of elongated particles in drug delivery applications has been realized with the advent of pioneering works of Discher's lab (Geng et. al., 2007; Geng and Discher, 2005).

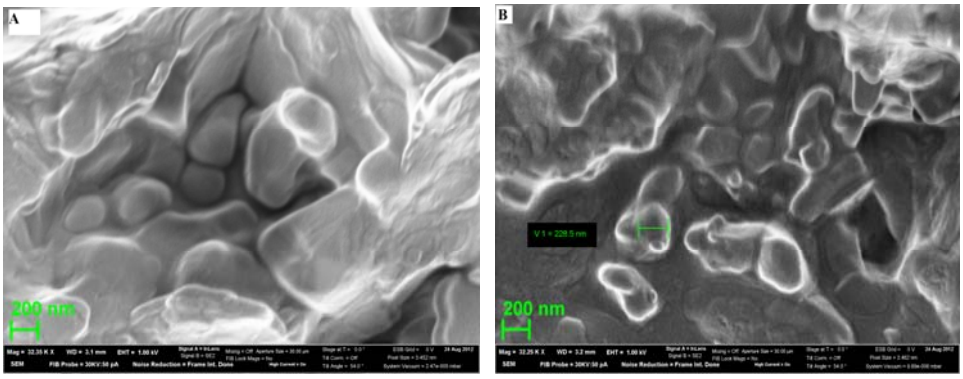

Fig 4. The SEM photographs of blank-NLC (A) and CMT loaded NLC (B).

3.4. Small-Angle Neutron Scattering

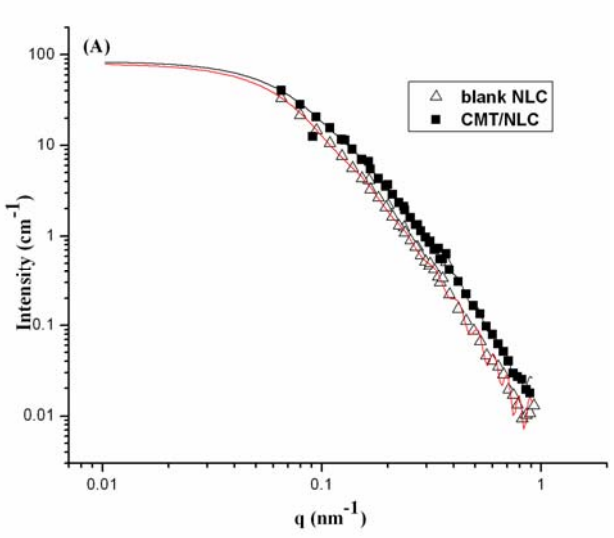

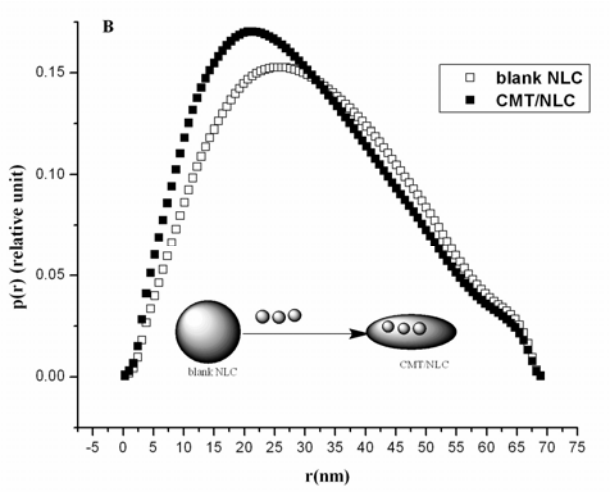

Fig 5. SANS spectra of NLC before and after loaded with CMT-3 in PBS (A); P(r) function obtained from the corresponding scattering curves in A.

SANS was used to study the effect of CMT-3 on the NLC structure. Indirect fourier transformation (IFT) method was applied in this study. This model-independent approach needs only minor additional (model) information on the possible aggregate structure (Glatter., 1977). The experimental data and the fitted curve coincide very well for both blank NLC and CMT/NLC for all q ranges (Fig 5A).

The possible shape and diameter can be obtained from the pair distance distribution p(r) function (Fig 5B). Blank NLC displayed almost spherical structure (maximum of p(r) function is located near the middle of maximal size), while after adding CMT-3 the maximum of p(r) moves to smaller r and it could be interpreted that the shape became elongated. In fact, this result is agreement with that of SEM. The particle size (mean diameter) obtained from Fig 5B was significantly smaller than the data got from DLS. There were two reasons for this disagreement: i) due to limited q_{min} SANS data point only on low limit of maximal size of aggregate, ii) DLS

observes hydrated size of particles (particles plus hydrated water) and SANS points to "dry size".

It is important to obtain the direct information about the structure change from the large q part of SANS measurements. At a q range, an evidence for fractals in the submicrometer and nanometer scale can be conveniently derived from small-angle scattering based on well-known dimensional analysis (Schmidt, 1995). The power law of the scattering intensity I(q) can be described as $I(q) \sim q^{-\alpha}$. This exponent indicates the microscopic structure of scatter can be understood as mass fractals or surface fractals. When the angular coefficient of the log I(q) versus log q plot is determined, its relationship with the dimensions of mass and surface fractal, Dv and Ds is $\alpha = 2 \times Dv - Ds$. In this study, the α values for blank NLC and CMT/NLC were 3.55 and 3.7, respectively. It means that such particles have a dense core and rough surface, the core has a Euclidean dimension, Dv=3, whereas the surface obey a relation $Ds = 6 - \alpha$. Decreasing of value of surface fractal dimension from 2.45 to 2.3 by adding drug to NLC points on changes of surface of NLC which become smoother. It was in qualitative agreement with SEM.

3.5. Small-Angle X-Ray Scattering

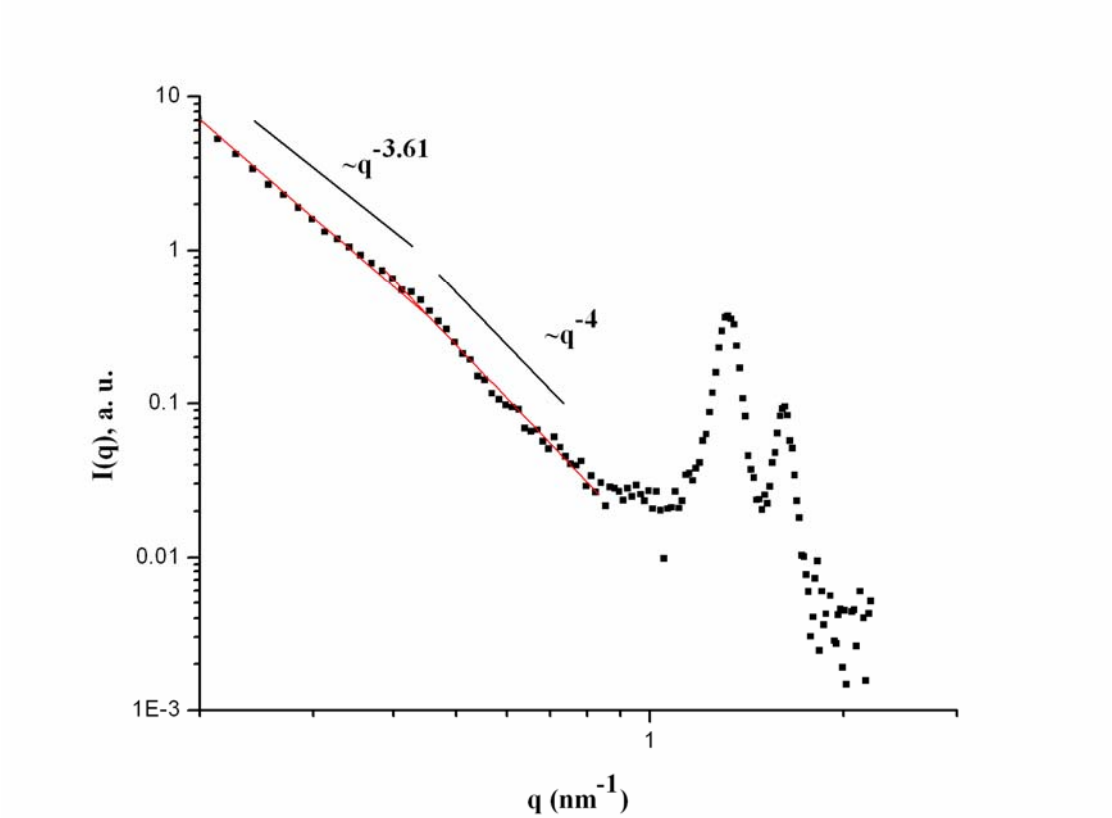

Fig 6. SAXS curve for film freeze-dried blank-NLC and CMT/NLC at 25 °C.

The three-dimensional structures of freeze-dried CMT/NLC and blank NLC were studied by SAXS. The evaluation of the X-ray spectra was got as reported before (Seydel et al., 1989; Mariani et al., 1993). There are two peaks (Fig 6, q = 1.31 nm^{-1}, 1.61 nm^{-1}), which means that CMT/NLC is cubic in 3-dimensional structures (Brandenburg et al., 1998). In fact, blank NLC had the same structures, thus the adding of CMT-3 did not change the 3-dimensional structures. Low q part of SAXS has been analyzed by dimensional analysis similar to SANS data obtained for solution of NLC. Slope of I(q) vs q points to surface fractal structure and corresponds to surface fractal dimension 2.39 similar to NLC in solution. For blank NLC, the slope varied from 3.71 to 3.88 at q=0.48 nm^{-1}(curve is not shown), which was coincided with the rough surface that got from SANS. In the case of CMT/NLC we have also

observed crossover from slope of 3.61 to 4 (smooth surface) at q=0.43 nm^{-1} which points on size of primary smooth aggregates forming fractal cluster around 2 nm.

3.6. Wide-Angle X-ray powder diffraction

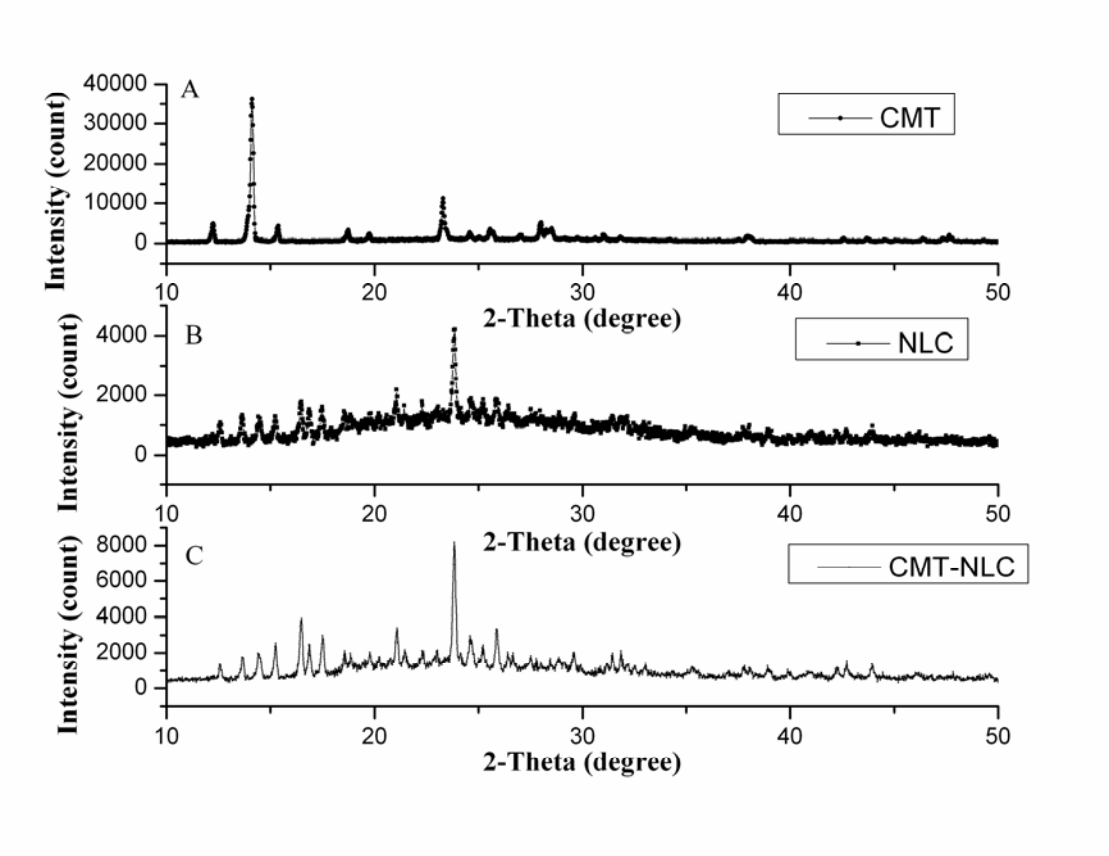

Fig 7. X-ray diffraction analysis of CMT-3 formulations: X-ray powder diffractograms of CMT-3 (A), freeze-dried unloaded blank-NLC (B) and freeze-dried CMT/NLC (C).

XRD was used to study changes of the microstructure in NLC. XRD analysis makes it possible to assess the length of the long and short spacing of the lipid lattice. In Fig 7, the intensities of several diffraction peaks characteristic of CMT-3 reduced in freeze-dried CMT/NLC, and the diffraction intensity of CMT/NLC was clearly

stronger than that of unloaded blank-NLC. This phenomenon could be attributed to crystal changes. Many factors can result in changes of crystal structure, for example, the amount and state of CMT-3 in NLC (Veerawat et al., 2008). Also, the differences in intensity between blank-NLC and CMT/NLC may be due to the less ordered microstructure of blank-NLC in comparison to that of CMT/NLC (Lopes et al., 2012). Thus, adding CMT-3 to imperfect NLC increases crystallinity of CMT/NLC.

3.7. In vitro release of CMT-3

The release experiment was conducted under sink conditions and the dynamic dialysis was used to separate the CMT-3 that released from CMT/NLC. Fig 8 demonstrated the influence of pH on release profiles of CMT/NLC and release rate of CMT-3 from CMT/NLC in PBS (0.5 % of Tween 80 in PBS, pH 7.4). It was obviously that about 58 % CMT-3 released from NLC in PBS (pH 5.6), while for PBS (pH 7.4) there was about 68 % CMT-3 released from NLC. Thus acidity seemed good for prolonged release, and CMT-3 had burst release in both medium. But in the following hours, CMT-3 showed prolonged release profiles. As for release rate (Fig 8B), the release rate of CMT-3 in PBS (pH 7.4) decreased sharply in the first 3 hours, but after the first 3 hours, the release rate was almost constant (0.02 mg/h) in the following 45 hours. Thus in both release medium, CMT/NLC exhibited a burst-prolonged release profile. The solid matrix of NLC and location of CMT-3 in NLC might attribute to this release pattern. It was reported that the drug can be incorporated between fatty acid chains, between lipid layers or in imperfections (Sylvia and Rainer., 2004). During the cooling process, solid lipids (SA and MGE)

rapidly solidified to form solid lipid core for their high melting points, and the rest liquid lipids distributed randomly around solid lipid core. As liquid lipids had higher solubility of drug, large amount of drug were loaded in outer lipid layer. In vitro-release experiment, in the burst release stage, CMT-3 that loaded in shell released easily and rapidly, while in the sustained release stage, the CMT-3 that loaded in solid lipid core released by matrix erosion and degradation of lipid components of NLC, which resulted in prolonged release manner. In addition, the cubic structure of CMT/NLC protected CMT-3 from leaking from NLC, Other factors contributing to the fast release are the large surface area, high diffusion coefficient of nanoparticles, the low viscosity, and short diffusion coefficient of CMT-3 and surfactant concentration (Zhigaltsev et al., 2010).

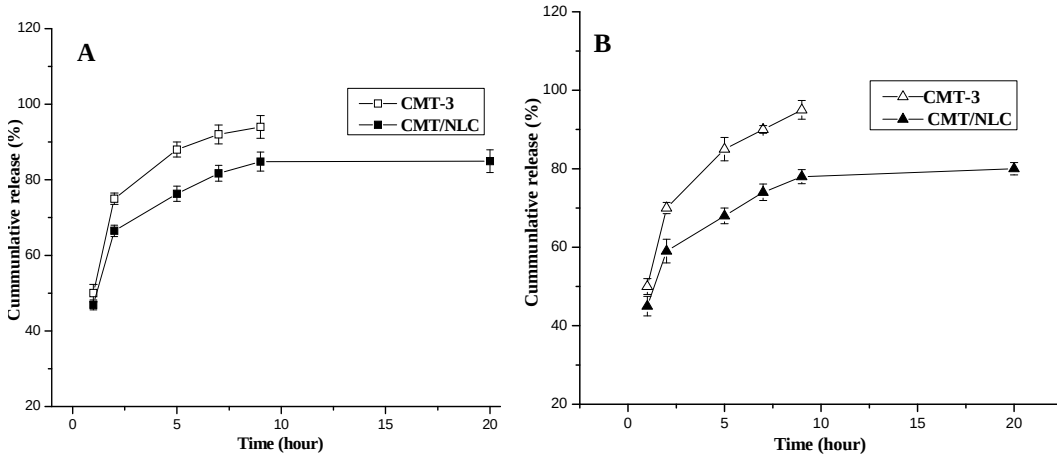

Fig 8. The in-vitro release study. Cumulative release of CMT-3 in different release mediums: pH7.4 (A), and pH5.6 (B). Values are mean ± SD (n=3).

3.8. In vitro cellular cytotoxicity assays

In order to know the biological activity of CMT-3 loaded nanoparticles (CMT/NLC), the cellular cytotoxicity was evaluated by MTT assay. As Fig 9 shows,

CMT-3 exhibits great inhibition effect on Hela cells growth in the given concentration. For example, the viability of HeLa cells treated with 20 μM CMT-3 for 24 h or 48 h was 70.9±7.5 % and 61.1±4.4 %, respectively. When treated with 20 μM CMT-3 for 24h, CMT/NLC had more inhibitory ability than CMT-3 ($t=3.02$, $P<0.05$, Fig 9A). Compared to CMT-3, the inhibition effects of CMT/NLC was also remarkably greater over concentration ranging from 2 to 20 μM when treated for 48 h ($t=6.00$, 4.40, 4.49, 25.55, $P<0.01$, Fig 9B), which means the sustained release properties of CMT/NLC for its cubic structure. It should be pointed out that blank-NLC did not have any obvious cytotoxicity on HeLa cells, even in high concentration and 48 h exposures.

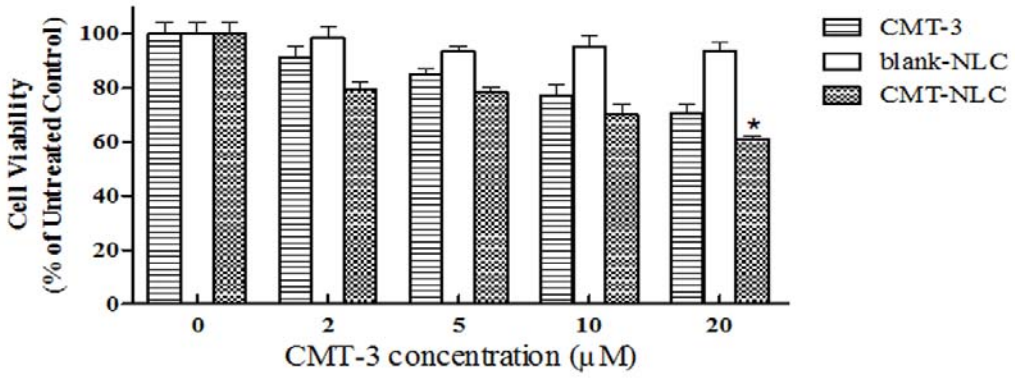

A.

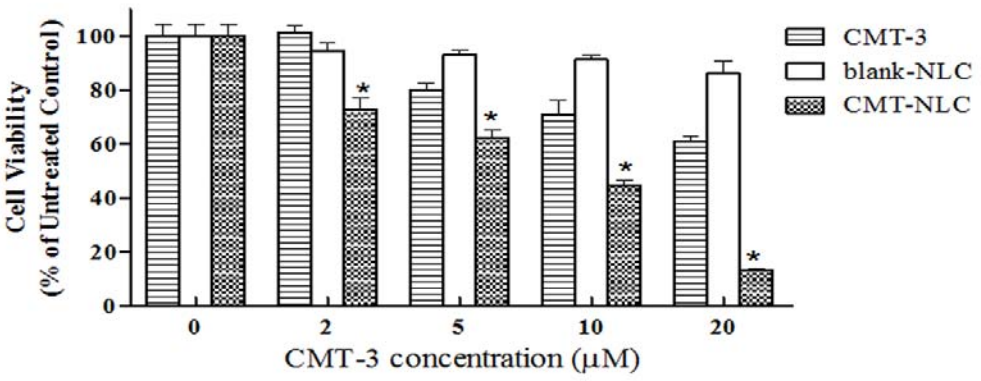

B.

Fig 9. In vitro cytotoxicity of CMT-3 and CMT/NLC against HeLa cells for 24 h (A) or 48 h (B). Cell viability is expressed as the percentage of untreated controls. Data

are given as mean±SD (n=6). *p < 0.05 compared with CMT-3.

3.9. Cell morphology

In order to compare the morphology changes of HeLa cells treated with CMT and CMT/NLC, we used the microscope and digital camera to observe the differences between the groups. 20 μM CMT-3 exhibits no obvious effect to HeLa cells' morphology for 6 h (Fig 10B), and the same phenomenon was observed when cells were treated with blank-NLC (Fig 10C), the volume of which was the same as CMT/NLC. But, CMT/NLC make cells' morphology changes a lot. As Fig 10D shows, cell condensation and fragmentation as well as cell shrinkage were observed. The results indicated that CMT/NLC was easier in leading to cells' toxicity compared to CMT-3 at the same concentration.

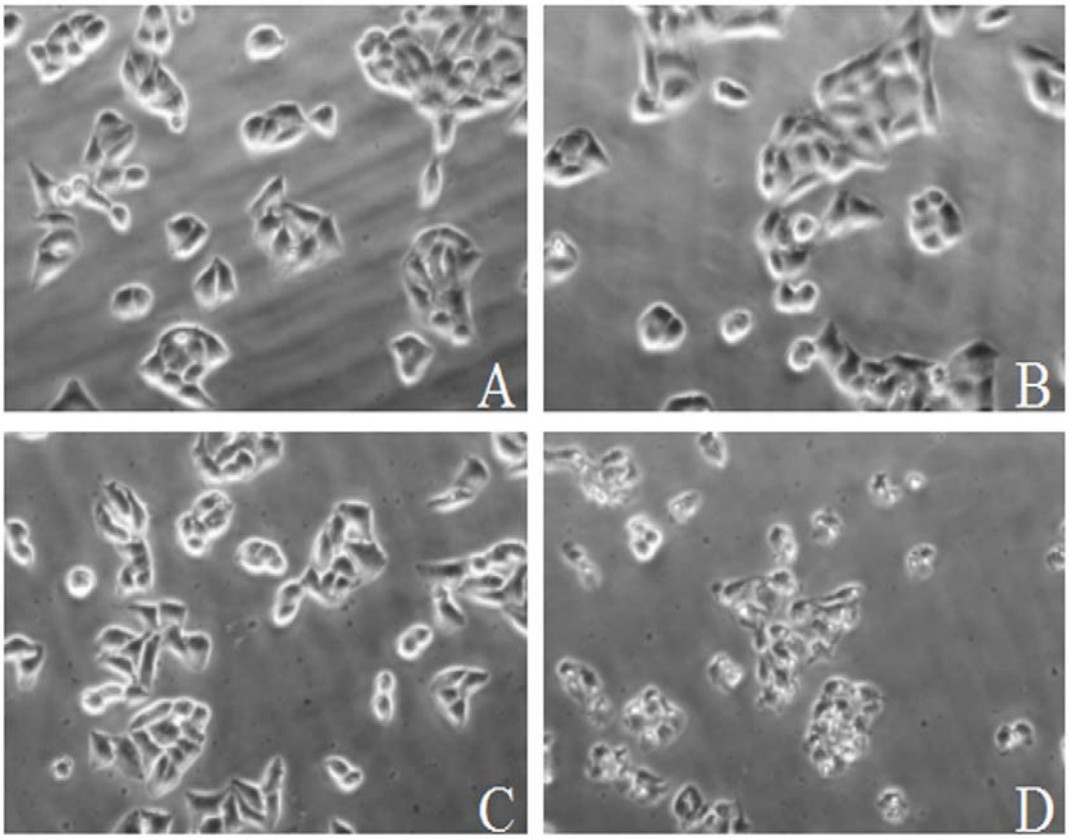

Fig 10. HeLa cells were treated with different medium for 6 h: A. control, without any treatment; B. 20 μM CMT-3; C. blank-NLC (same volume with CMT/NLC); D. CMT/NLC (CMT concentration is 20 μM). Cells were captured by digital camera (×200).

3.10. Cellular uptake of NLC formulations

We observed the changes of HeLa cells' morphology after treated with RB/NLC. After HeLa cells were exposed to RB/NLC for 2 h (Fig 11 row 1B shows), it was clearly that some white pellets appeared around the cells, it was assumed to be RB/NLC. The control group without CMT/NLC treatment (Fig 11 row 1A shows) has no this phenomenon.

In order to observe the intracellular distribution of NLC, Cell'R Live Cell Station was used to capture Hela cells after treatment with RB/NLC every 30 second. As time went on, the intensity of fluorescence was increasing in cytoplasm in HeLa cell. As shown in Fig 11 rows 2 - 3, the fluorescence of rhodamine B became obvious at 9 min when treated with RB/NLC. These demonstrated that RB/NLC can enter into cell's cytoplasm quickly. In fact, it is realized that many therapeutics (e.g. anti-cancer drugs, photosensitizers and anti-oxidants) and biotherapeutics (e.g. peptide and protein drugs, DNA and siRNA) have to be delivered and released into the cellular compartments such as the cytoplasm or cell nucleus, in order to exert therapeutic effects (Torchilin., 2006; Nori et al., 2005).

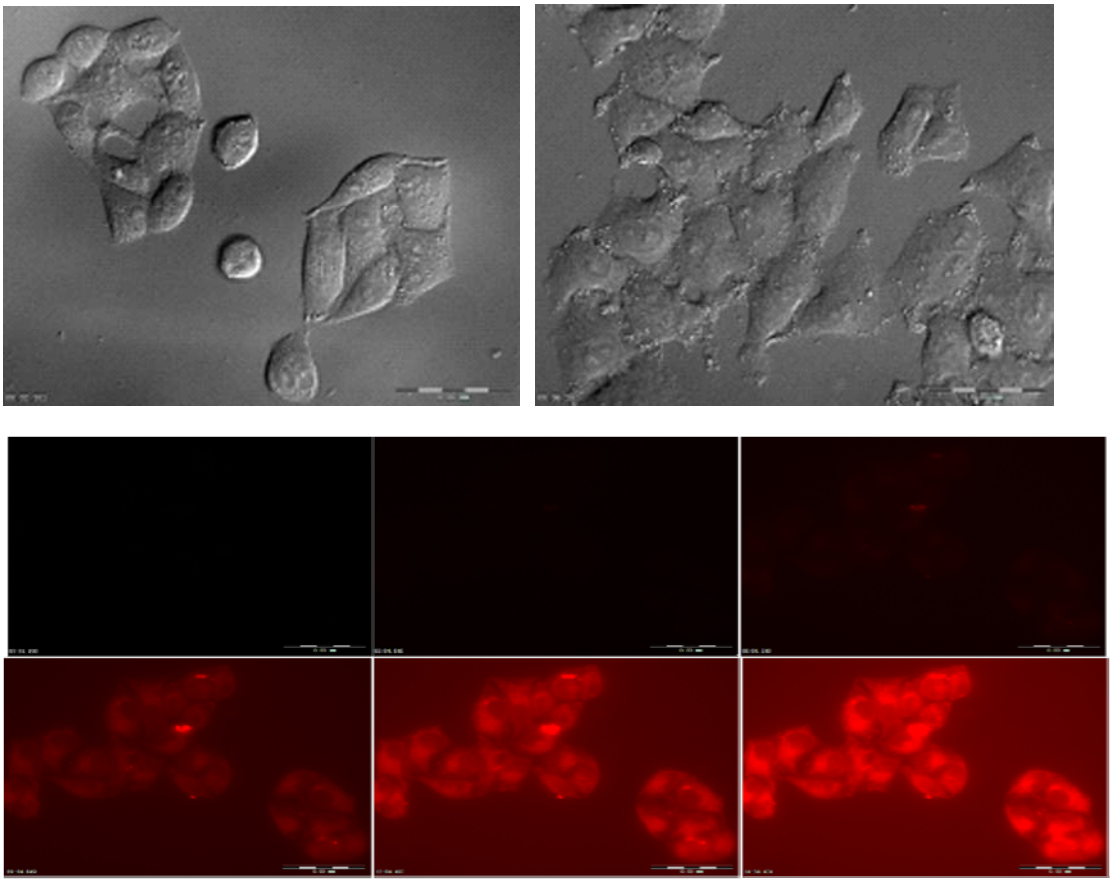

Fig 11. R1(A): control, without RB-NLC treatment; R1(B): HeLa cells were treated with RB-NLC for 2 h; R2, 3: Red fluorescence from Rhodamine B, where the Hela cells incubated with RB/NLC at the time of 0, 3, 6, 9,12, 15 minutes, respectively. All images were captured by Cell'R Live Cell Station (×60).

4. Conclusion

A system of the NLC, *i.e*. nanostructured lipid carrier, was successfully developed in this study for controlled and sustainable delivery of anticancer drugs with CMT-3 as a model drug. The ratios between lipids, drug and surfactants and lipid types, were studied for their effect on long term stability and uniformity of nanoparticles size distribution. The NLC particle size (diameter) was about 150 nm

during the 30 days observation period with about 90% encapsulation efficiencies. SANS showed that CMT/NLC owns smoother surface than blank NLC. And the shapes of CMT/NLC become elongated, which coincided to SEM result. The 3-dimensional structures of CMT/NLC and blank NLC were cubic according to the results of SAXS, which was suspected to attribute the burst-sustained release model of CMT/NLC. The in vitro cellular cytotoxicity assay (MTT) data suggested that NLC was not cytotoxic to HeLa cells under test conditions, but that CMT/NLC was more cytotoxic than CMT at the same drug concentration. The increased toxicity of CMT/NLC was attributed to the increased solubility of CMT-3, a hydrophobic anticancer drug, in the CMT/NLC formulation. More time exposures resulted in higher cellular cytotoxicity was agreement with the sustained release properties of CMT/NLC. Moreover, the possible location of NLC at cytoplasm should also be favorable to the cytotoxicity improvement of CMT-3. Of course, the exploration of nano-material carrier to fit CMTs still has a lot of work to do, which will be our next further research plan.

Acknowledgment

We would like to express our gratitude to Prof. Leonard I Wiebe for thoughtful discussions. A. Z. gratefully acknowledges the support of this work by the Alexander von Humboldt Foundation. We gratefully acknowledge the support of this work by Chinese National Natural Science Foundation (201003047) and Fundamental Research Funds for the Central Universities (WK1014024). SANS measurements

have been performed under the support of the European Commission (Grant agreement N 226507-NMI3). Laszlo Almasy is acknowledged for help during SANS measurements. Daniel Laipple is acknowledged for help during SEM measurements.

References

Brandenburg, K., Richter, W., Koch, M.H.J., Meyer, H.W., Seydel, U., 1998. Characterization of the nonlamellar cubic and H_{II} structures of lipid A from Salmonella enterica serovar Minnesota by X-ray diffraction and freeze-fracture electron microscopy. Chem.Phys.Lipids. 91, 53-69.

Delmas, T., Couffin, A.C., Bayle, P.A., Crecy, F., Neumann, E., Vinet, F., Bardet, M., Bibette, J., Texier, I., 2011. Preparation and characterization of highly stable lipid nanoparticles with amorphous core of tuneable viscosity. Colloid Interface Sci. 360, 471-481.

Dreiss, C. A., 2007. Wormlike micelles: Where do we stand? Recent developments, linear rheology and scattering to techniques. Soft Matter. 956-970.

Eliana, B.S., Rainer, M.H., 2010. Lipid Nanoparticles: Effect on Bioavailability and Pharmacokinetic Changes. Drug delivery. 115-134.

Ezrahi, S., Tuval, E., Aserin, A., 2006. Properties, main applications and perspectives of worm micelles. Adv. Colloid Interface Sci. 77-102.

Geng. Y., Discher. D. E., 2005. Hydrolytic degradation of poly(rthylene oxide)-block-poly(caprolactone) worm micelles. J. Am. Chem. Soc.12780-12781.

522 Geng. Y., Dalhaimer. P., Cai. S., Tsai. R., Tewari. M., Minko. T., Discher. D.E., 2007.
523 Shape effects of filaments versus spherical particles in flow and drug delivery. Nat,
524 Nanotechnol. 249-255.

525 Glatter. O., 1977. A new method for the evaluation of small-angle scattering data. J.
526 Appl. Cryst. 10, 415-421.

527 Golub, L.M., Ramamurthy, N.S., McNamara, T.F., Greenwald, R.A., Rifkin, B.R.,
528 1991. Tetracyclines inhibit connective tissue breakdown: new therapeutic
529 implications for an old family of drugs. Crit Rev Oral Biol Med. 2, 297-321.

530 Gu, Y., Lee, H.M., Roemer, E.J., Musacchia, L., Golub, L.M., Simon, S.R., 2001.
531 Inhibition of tumor cell invasiveness by chemically modified tetracyclines. Curr
532 Med Chem. 8, 261–270.

533 Ji, J.G., Wu, D.J., Liu, L., Chen, J.D., Xu, Y., 2012. Preparation, characterization, and
534 in vitro release of folic acid-conjugated chitosan nanoparticles loaded with
535 methotrexate for targeted delivery. Polym. Bull. 68, 1707-1720.

536 Khalil, M., Ranjita, S., Sven, G., Cecilia, A., Rainer, M.H., 2011. Lipid nanocarrier for
537 dermal delivery of lutein: Prepartion, characterization, stability and performance.
538 Int J Pharm. 414, 267-275.

539 Patricia, S., Samantha, C.P., Eliana, B.S., Maria, H.A.S., 2011. Polymorphism,
540 crystallinity and hydrophilic-lipophilic balance of stearic acid and stearic
541 acid-capric/caprylic triglyceride matrices for production of stable nanoparticles.
542 Colloid and Surface B: Biointerfaces. 86, 125-130.

543 Lokeshwar, B.L., Selzer, M.G., Zhu, B.Q., Block, N.L., Golub, L.M., 2002. Inhibition
544 of cell proliferation, invasion, tumor growth and metastasis by an oral
545 non-antimicrobial tetracycline analog (COL-3) in a metastatic prostate cancer
546 model. Int J Cancer. 98, 297-309.

547 Lokeshwar, B.L., 1999. MMP inhibition in prostate cancer. Ann N Y Acad Sci. 878,
548 271–289.

549 Lokeshwar, B.L., Houston-Clark, H.L., Selzer, M.G., Block, N.L., Golub, L.M., 1998.
550 Potential application of a chemically modifiednon-antimicrobial tetracycline
551 (CMT-3) against metastatic prostate cancer. Adv Dent Res. 12, 97–102.

552 Lokeshwar, B.L., Escatel, E., Zhu, B., 2001. Cytotoxic activity and inhibition of
553 tumor cell invasion by derivatives of a chemically modified tetracycline CMT-3
554 (COL-3). Curr Med Chem. 8, 271–279.

555 Lokeshwar, B.L., Selzer, M.G., Zhu, B.Q., Block, N.L., Golub, L.M., 2002. Inhibition
556 of cell proliferation, invasion, tumor growth and metastasis by an oral
557 non-antimicrobial tetracycline analog (COL-3) in a metastatic prostate cancer
558 model. Int J Cancer.98, 297–309.

559 Lopes, R., Eleuterio, C.V., Goncalves, L.M.D., Cruz, M.E.M., Almeida, A.J., 2012.
560 Lipid nanoparticles containing oryzalin for the treatment of leishmaniasis. Eur J
561 Pharm Sci. 45, 442-450.

562 Liu, Y., Wang, P.F., Sun, C., Feng, N.P., Zhou, W.X., Yang, Y., Tan, R., Chen, Z.Q.,
563 Wu, S., Zhao, J.H., 2010. Wheat grem agglutinin-grafted lipid nanoparticles:

564 Preparation and in vitro evaluation of the association with Caco-2 monolayers. Int J
565 Pharm. 397, 155-163.

566 Mariani, P., Luzzati, V., Delacroix, H., 1993. Cubic phases of lipid-containing
567 systems. Structure analysis and biological implications. J. Mol. Biol. 204, 165-189.

568 Medha, D.J., Rainer, M.H., 2009. Lipid nanoparticles for parenteral delivery of
569 actives. Eur J Pharm Biopharm. 71, 161-172.

570 Meng, Q., Xu, J., Goldberg, I.D., Rosen, E.M., Greenwald, R.A., Fan, S., 2000.
571 Influence of chemically modified tetracyclines on proliferation, invasion and
572 migration properties of MDA-MB-468 human breast cancer cells. Clin Exp
573 Metastasis.18, 139-46.

574 Nori, A., Kopecek, J., 2005. Intracellular targeting of polymer-bound drugs for cancer
575 chemotherapy. Adv. Drug. Deliv. Rev. 57, 609-636.

576 Nukolova, N.V., Oberoi, H.S., Cohen, S.M., Kabanov, A.V., Bronich, T.K., 2011.
577 Folate-decorated nanogels for targeted therapy of ovarian cancer. Biomaterials. 32,
578 5417-5426.

579 Radheshyam, T., Kamla, P., 2011. Nanostructured lipid carrier versus solid lipid
580 nanoparticles of simvastain: Comparative analysis of characteristics,
581 pharmacokinetics and tissues uptake. Int J Pharm. 415, 232-243.

582 Rainer, M.H., 2007. Lipid nanoparticles: recent advances. Adv Drug Deliv Rev. 59,
583 375-376.

584 Rainer, M.H., Cornelia, M.K., 2004. Challenges and solutions for the delivery of

585 biotech drugs-a review of drug nanocrystal technology and lipid nanoparticles. J of
586 Biotechnology. 113, 151-170.

587 Rosta L., 2002. Cold neutron research facility at the Budapest Neutron Centre. Appl
588 Phys. A. 74, S292-S294.

589 Schmidt, P. W., 1995. Some Fundamental Concepts and Techniques Useful in
590 Small-Angle Scattering Studies of Disordered Solids. In Modern Aspects of
591 Small-Angle Scattering; Brumberger, H., Ed.; Kluwer Academic Publishers: The
592 Netherlands, pp 1-56.

593 Seftor, R.E., Seftor, E.A. De, Larco, J.E., Kleiner, D.E., Leferson, J.,
594 Stetler-Stevenson, W.G., McNamara, T.F., Golub, L.M., Hendrix, M.J., 1998.
595 Chemically modified tetracyclines inhibit human melanoma cell invasion and
596 metastasis. Clin Exp Metastasis. 16, 217-25.

597 Selzer, M.G., Zhu, B., Block, N.L., Lokeshwar, B.L., 1999. CMT-3, a chemically
598 modified tetracycline, inhibits bony metastases and delays the development of
599 paraplegia in a rat model of prostate cancer. Ann N Y Acad Sci. 878, 678–682.

600 Soheila, K., Ebrahim, V.F., Mohsen, N., Fatemeh, A., 2010. Preparation and
601 characterization of ketoprofen-loaded solid lipid nanoparticles made from beeswax
602 and carnauba wax. Nanomedicine: Nanotechnology, Biology, and Medicine. 6,
603 753-759.

604 Seydel, U., Brandenburg, K., Koch, M.H.J., Rietschel, E.T., 1989. Supramolecular
605 structure of lipopolysaccgaride and free lipid Aunder physiological conditions as

606 determined by synchrotron small-angle X-ray diffraction. Eur. J. Biochem. 186,
607 325-332.

608 Syed S, Takimoto C, Hidalgo M, Rizzo J, Kuhn JG, Hammond LA, Schwartz G,
609 Tolcher A, Patnaik A, Eckhardt SG, Rowinsky EK. A phase I and pharmacokinetic
610 study of Col-3 (Metastat), an oral tetracycline derivative with potentmatrix
611 metalloproteinase and antitumor properties. Clin Cancer Res. 2004;
612 10(19):6512-21.

613 Sylvia, A.W., Rainer, M.H., 2004. Solid lipid mamoparticles for parenteral drug
614 delivery. Adv Drug Deliv Rev. 56, 1257-1272.

615 Torchilin, V.P., 2006. Recent approaches to intracellular delivery of drugs and DNA
616 and organelle targeting. Annu. Rev. Biomed. Eng. 8, 343-375.

617 Veerawat, T., Prapaporn, B., Eliana, B.S., Rainer, M.H., Varaporn, B.J., 2008.
618 Influence of oil content on physicochemical properties and skin distribution of Nile
619 red-loaded NLC. J Control Release. 128, 134-141.

620 Venkateraman, S., Hedrick, J.L., Ong, Z.Y., Yang, C., Ee, P.L.R., Hammond, P.T.,
621 Yang, Y.Y., 2011. The effects of polymeric nanostructure shape on drug delivery.
622 Adv Drug Deliv Rev. 63, 1228-1246.

623 Wang, J.J., Liu, K.S., Sung, K.C., Tsai, C.Y., Fang, J.Y., 2009. Lipid nanoparticles
624 with different oil/fatty eater ratios as carrier of buprenorphine and its prodrugs for
625 injection. Eur. J. Pharm. Sci. 38, 138-146.

626 Xu, Z.H., Chen, L.L., Gu, W.W., Gao,Y., Lin, L.P., Zhang, Z.W., Xi, Y., Li, Y.P., 2009.

The performance of docrtaxel-loaded solid lipid nanoparticles targeted to hepatocellular carcinoma. Biomaterial. 30, 226-232.

Yoo, J.W., Doshi, N., Mitragotri, S., 2011. Adaptive micro and nanoparticles: Temporal control over carrier properties to facilitate drug delivery. Adv Drug Deliv Rev. 63, 1247-1256.

Zhigaltsev, I.V., Winters, G., Srinivasulu, M., Crawford, J., Wong, W., Amankwa, L., 2010. Development of a weak-base docetaxel derivative that can be loaded into lipid nanoparticles. J Control Release. 144, 332-340.

Figure Legends

646 **Figure 1.** The structures of doxycycline (upper) and CMT-3 (lower).

647 **Fig 2.** The effects of lipids and CMT-3 concentration on entrapment efficiency and
648 drug loading. *The labels of samples are the same as in Table. 3. Values are mean ±
649 SD (n=3).

650 **Fig 3.** AFM images of blank-NLC (A), and CMT/NLC (B).

651 **Fig 4.** The SEM photographs of blank-NLC (A) and CMT loaded NLC (B).

652 **Fig 5.** SANS spectra of NLC before and after loaded with CMT-3 in PBS (A); P(r)
653 function obtained from the corresponding scattering curves in A.

654 **Fig 6**. SAXS curve for film freeze-dried blank-NLC and CMT/NLC at 25 °C.

655 **Fig 7.** X-ray diffraction analysis of CMT-3 formulations: X-ray powder
656 diffractograms of CMT-3 (A), freeze-dried unloaded blank-NLC (B) and freeze-dried
657 CMT/NLC (C).

658 **Fig 8.** The in-vitro release study. Cumulative release of CMT-3 from CMT/NLC in
659 different release mediums (A, Values are mean ± SD (n=3)), and average release rate
660 of CMT-3 from CMT/NLC in pH release medium (B).

661 **Fig 9.** In vitro cytotoxicity of CMT-3 and CMT/NLC against HeLa cells for 24 h (A)
662 or 48 h (B). Cell viability is expressed as the percentage of untreated controls. Data
663 are given as mean±SD (n=6). *$p < 0.05$ compared with CMT-3.

664 **Fig 10.** HeLa cells were treated with different medium for 6 h: A. control, without any
665 treatment; B. 20 μM CMT-3; C. blank-NLC (same volume with CMT/NLC); D.
666 CMT/NLC (CMT concentration is 20 μM). Cells were captured by digital camera

(×200).

Fig 11. R1(A): control, without RB-NLC treatment; R1(B): HeLa cells were treated with RB-NLC for 2 h; R2, 3: Red fluorescence from Rhodamine B, where the Hela cells incubated with RB/NLC at the time of 0, 3, 6, 9,12, 15 minutes, respectively. All images were captured by Cell'R Live Cell Station (×60).

Table legends

689 **Table 1.** Effects of lipid ingredients on mean particle size of blank-NLC.

690 **Table 2.** Effects of the concentration of surfactants on mean particle size and stability.

691 **Table 3.** The effects of lipids and CMT-3 content on mean particle size. Values are

692 mean ± SD (n=3)

693